SERBIAN JOURNAL OF ELECTRICAL ENGINEERING
Vol. 9, No. 3, October 2012, 343-359

UDK: 621.313.333:621.311.245 **DOI: 10.2298/SJEE1203343B**

Autonomous SEIG in a Small Wind Power Plant with Voltage and Frequency Control

Azzeddine Benlamoudi[1], Rachid Abdessemed[2]

Abstract: This paper deals with the application of an autonomous Self-Excited Induction Generator (SEIG) in a small wind power conversion system (WPCS). Such conversion system has capability to supply power demand of the loads with constant voltage and frequency, for which a power managing method is proposed. Voltage Sourced Converter (VSC) along with Battery Energy Storage System (BESS) is used to handle power flow between the SEIG and loads. The proposed control scheme, using a single voltage closed-loop control, is found to be suitable to regulate both voltage and frequency. The WPCS is modelled in MATLAB/Simulink and Power System Block-set (PSB). Simulation results show that Voltage Frequency Controller (VFC) has ability to keep the voltage and frequency constant in spite of perturbations.

Keywords: Voltage Frequency Controller (VFC), Self-Excited Induction generator (SEIG), Battery Energy Storage System (BESS), Wind Power Conversion System (WEPS).

1 Introduction

Due to climate changes such as temperature rise due to increase in greenhouse gases (GHG) emission, increase in sea level, high oil price, depletion of fossil fuel reserves and growing in power demand, the world is obliged to search for new sources of energy on which the emission of GHG would be reduced to 5% from their 1990 level. These problems lead scientists towards new clean power conversion systems. The replenished energy resources are suitable to meet the clean power restrictions. Wind became an environmental-friendly and economically viable energy source.

Self-excited induction generators (SEIG) are reported to be suitable for small scale wind power plants [1, 2] because of their advantages such as low price, robustness, ease of maintenance, self-protection, easy maintainability, availability and capability to produce electrical power even at variable speed [3, 4]. These may be operated on/off grid-connected. In off grid mode or

[1]LRPI Industrial Prevention Research Laboratory, Institute of Health and Safety, University el Hadj Lakhdar Batna – Algeria, Cité 126 Logts Bloc 5 No. 42 Batna 05000, Algeria; E-mail: benlamoudia@gmail.com
[2]LEB Research Laboratory, Department of Electrical Engineering, University of Batna – Algeria, Avenue Chahid Med el Hadi Boukhlouf, 05000 Batna, Algeria; E-mail: rachid.abdessemed@gmail.com

Autonomous Wind Power Conversion System (AWPCS), SEIG is useful for supplying remote areas such as islands, military equipment, ships and small villages far from conventional resources. Major drawbacks in using SEIG are their poor voltage frequency regulation which depends upon generator speed, the amount of reactive power and the load nature. Literature provides information on several attempts that have been made to analyse the steady state, dynamic and transient behaviour of SEIG based standalone wind energy system [5 – 7]. To maintain constant output power at load terminals, many researchers have suggested control strategies and application of different power conditioning systems [8 – 11] for SEIG terminal voltage and frequency control. In the recent literature [12 – 18], the Battery Energy Storage System (BESS) with a Voltage Source Converter (VSC) is employed for isolated system. Methods have been proposed to regulate both the SEIG terminal voltage and frequency using two loop control [14 – 18]. In [19, 20] an investigation has been carried out using modulation index to control the terminal voltage and load angle to control the system frequency. To minimize the number of control loops, a single-loop control was proposed in [21].

In the present work, an attempt has been made to control the terminal voltage and frequency of an autonomous SEIG driven by a wind turbine. Voltage at the point of common coupling PCC is controlled by modulation index '*m*', while system frequency is imposed by VFC at the desired frequency by forcing phase angle of the VFC 'delta' at a desired value so that a single closed-loop control is used. VFC supplies reactive power demand of balanced loads and behaves as a power balancing system to adequately manage the power flow between the SEIG, BESS and power demand of the loads. This paper is organized as follows. The description of the wind energy conversion system is presented in Section 2. The operation principle of the proposed system is reviewed in Section 3. The control strategy is described in Section 4. Modelling of the WPCS is fulfilled in Section 5. Simulation results and analysis are provided in Section 6. Section 7 is the conclusion.

2 Description of Wind Power Conversion System

Fig. 1 shows schematic diagram of the system under study. The wind turbine is connected to the induction generator shaft through a step-up gear box. The excitation capacitor bank connected in delta and consumer loads is connected across the generator stator terminals. VFC, which consists of a combination of a VSC along-with BESS at its DC link side, is connected to the PCC. The purpose of the BESS is to improve WPCS stability. The proposed VFC acts as a bidirectional source of the active/reactive power. So it can control the terminal voltage magnitude and frequency, following both speed and load perturbations.

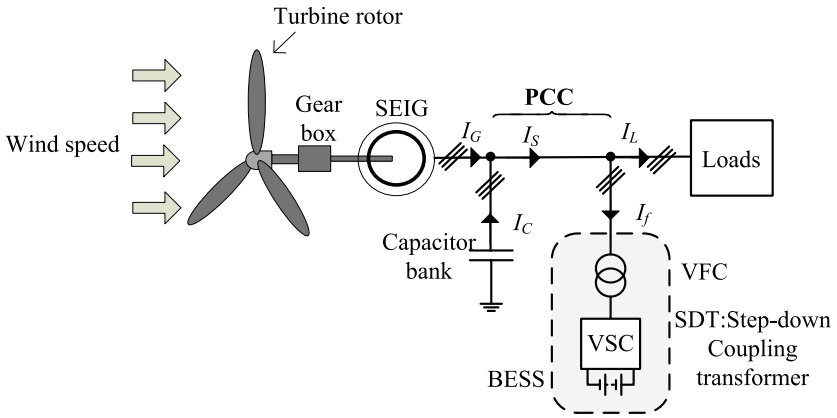

Fig. 1 – *Schematic diagram of the wind energy conversion system.*

3 Operation Principle

The WPCS is intended to supply power to linear/dynamic loads with a fixed voltage and frequency in variable operating conditions. The WPCS provided its rated active power P_{turb_R} reduced of the induction generator and gear-box losses, when the wind speed reaches its rated value V_{wind_R}. The change in active/reactive power flow causes the change in voltage and frequency at PCC. The VFC has the capability for maintaining the voltage and frequency constant regardless of the conditions of use. If the total load active power 'P_{load}' decreases, the generator active power P_{gen} decreases. Consequently, the terminal voltage and system frequency increase since the rotor speed is not regulated. On the other hand, if P_{load} increases P_{gen} increases also, the terminal voltage and frequency decrease as described in [18]. In other words, if P_{load} is less than the power provided by the generator P_{gen}, the VFC absorbs the power difference and stores the excessive energy in the 'BEES'; charging mode, the total reactive power Q_{load} is supplied by the VFC. Furthermore, if P_{load} is higher than P_{gen}, the VFC provides the power difference to compensate this gap, the BESS is in discharging mode, the total reactive power Q_{load} is remain supplied by the VFC. In the case when P_{gen} is equal to P_{load}, the VFC supplies solely reactive power to the load; the BEES is in stand-by mode. If the wind speed becomes less than the cut-in speed and the state of charge (SOC) of the BESS is slightly less than 100 %, the VFC automatically becomes the sole source to supply power to the load for a few hours.

4 Control Strategy

As shown in Fig. 1, the VSC is a major part in the WPCS, which interfaces the SEIG, the BESS and the loads it can keep the power balance to maintain the SEIG terminal voltage and frequency constant. The active and reactive power handling by the VFC are achieved by its intrinsic parameters; the modulation index '*m*' and the load angle 'δ'. Fig. 2 depicts the per phase equivalent circuit of the VFC connected to PCC through a coupling impedance. The exchanged power between the VFC and the PCC is described as [22]:

$$\begin{aligned} P + \mathrm{j}Q = \underline{S} = \underline{V}_G \underline{I}^* = \underline{V}_G \left(\frac{\underline{V}_G - \underline{V}_{PWM}}{\underline{Z}} \right)^* = \\ = V_G \left(\frac{V_G - V_{PWM}\, \mathrm{e}^{\mathrm{j}\delta}}{Z\, \mathrm{e}^{-\mathrm{j}\theta}} \right) = \frac{V_G^2}{Z} \mathrm{e}^{\mathrm{j}\theta} - \frac{V_G V_{PWM}}{Z} \mathrm{e}^{\mathrm{j}(\delta+\theta)}. \end{aligned} \tag{1}$$

Thus, active and reactive powers are described as follows:

$$P = \frac{V_G^2}{Z} \cos\theta - \frac{V_G V_{PWM}}{Z} \cos(\delta + \theta), \tag{2}$$

$$Q = \frac{V_G^2}{Z} \sin\theta - \frac{V_G V_{PWM}}{Z} \sin(\delta + \theta), \tag{3}$$

where $\underline{Z} = R + \mathrm{j}X$. Equations (2) and (3) are rewritten as:

$$P = \frac{V_G^2}{Z} \left[R V_G - V_{PWM} (R \cos\delta - X \sin\delta) \right], \tag{4}$$

$$Q = \frac{V_G^2}{Z} \left[X V_G - V_{PWM} (R \sin\delta + X \cos\delta) \right]. \tag{5}$$

For very small values R may be neglected, and if δ is less than 10°, then $\sin\delta \approx \delta$ and $\cos\delta \approx 1$.

Equations (4) and (5) become:

$$P = \frac{V_G V_{PWM}}{X} \delta, \tag{6}$$

$$Q = \frac{V_G}{X} (V_G - V_{PWM}) = \frac{V_G}{X} \Delta V, \tag{7}$$

where ΔV is voltage difference. Equations (6) and (7) show that the active power depends on the load angle δ, while the reactive power depends on the voltage difference ΔV. The magnitude voltage $|V_{\mathrm{PWM}}|$ is directly related to the modulation index *m*, according to the PWM control, as follows:

$$\left|V_{PWM}\right| = m\frac{V_{dc}}{2}. \tag{8}$$

When the voltage difference ΔV changes the voltage controller generates the required modulation index m in order to minimize the voltage difference. So, when $|V_G|$ decreases, the modulation index is increased; consequently $|V_{PWM}|$ increases. Indeed, the VFC supplies more reactive power to the SEIG. Therefore, the magnitude voltage $|V_G|$ increase.

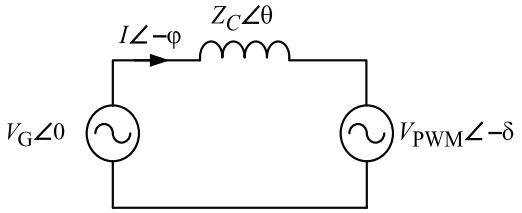

Fig. 2 – *Power flow between* SEIG *and* VFC *through coupling impedance.*

As described in Section 3, any frequency change is due the SEIG active power variation. Hence, to impose a constant frequency for a given rotor speed, the VFC must ensure the load active power demand so the real power flow remains constant. For such purpose, the load angle δ is fixed at a desired value corresponding at system frequency which is $\delta = \omega_s t = 2\pi f_s t$.

5 Wind Power Conversion System Modelling

The main components of the proposed WPCS are shown in Fig. 1. It consists of a horizontal axis wind turbine (HAWT), the SEIG, the VSC, the BESS and consumer loads. Modelling and simulation is done in MATLAB using PSB toolbox. The dynamic model of these subsystems is explained in the following subsections.

5.1 Modelling of wind turbine

The mechanical input torque T_t developed by the wind turbine using the power coefficient based on is given by:

$$T_t = 0.5\rho\pi R^3 \frac{C_p(\lambda,\beta)}{\lambda} v_w^2, \tag{9}$$

Where:

C_p – power coefficient of the wind turbine;
ρ – air density (1,225 [kg/m^3] in standard atmosphere);
R – radius of the wind turbine [m];
v – wind speed [m/s];
β – pitch angle [°];

λ – tip speed ratio TSR.

The tip speed ratio is defined as the ratio of the linear speed at the tip of the blade ($\Omega_t R$) and the wind speed, Ω_t being the rotational speed of the wind turbine and related at the rotational speed of the generator (Ω_r) by the gain (G) of the step-up gear box as:

$$\lambda = \frac{\Omega_t R}{v_w} = \frac{\Omega_r R}{v_w G}. \tag{10}$$

A generic equation to model the $C_p(\lambda, \beta)$ characteristic of the wind turbine [5] is presented as:

$$C_p(\lambda,\beta) = c_1\left(\frac{c_2}{\lambda_i} - c_3\beta - c_4\right)\mathrm{e}^{\frac{-c_5}{\lambda_i}} + c_6\lambda, \tag{11}$$

$$\frac{1}{\lambda_i} = \frac{1}{\lambda + 0.08\beta} - \frac{0.035}{\beta^3 + 1}. \tag{12}$$

Fig. 3 shows the power coefficient versus tip speed ratio at a zero degree pitch angle. It shows that C_p reaches a maximum value $C_{p\,\max} = 0.48$ for a tip speed ratio $\lambda_{opt} = 8.1$, which yields the optimum wind turbine torque and the maximum mechanical power available in the wind turbine for a given wind speed. At a rated wind speed 11 m/s, the SEIG develops the maximum power and generates the rated voltage at rated frequency.

5.2 Modelling of self-excited induction generator

The dynamic model of the SEIG is developed based on the well-known simplifying assumptions and on the saturation effect.

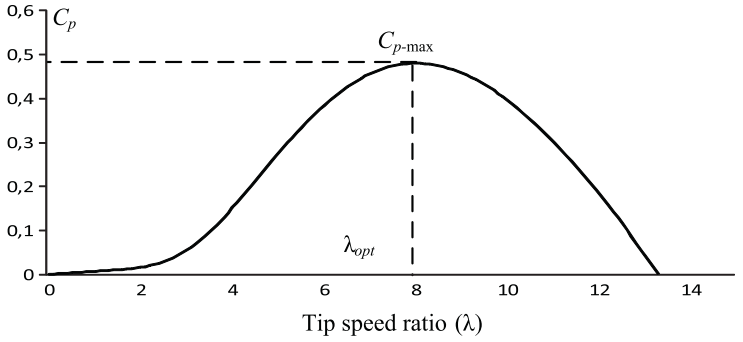

Fig. 3 – *Power coefficient versus tip speed ratio (pitch angle* $\beta = 0$).

The mathematical model of SEIG in stationary d-q axis reference frame is described by the following equations:

$$v_{sd} = R_s i_{sd} + \frac{\mathrm{d}}{\mathrm{d}t}\varphi_{sd}, \tag{13}$$

$$v_{sq} = R_s i_{sq} + \frac{\mathrm{d}}{\mathrm{d}t}\varphi_{sq}, \tag{14}$$

$$0 = R_r i_{rd} + \frac{\mathrm{d}}{\mathrm{d}t}\varphi_{rd} + \omega_r \varphi_{rq}, \tag{15}$$

$$0 = R_r i_{rq} + \frac{\mathrm{d}}{\mathrm{d}t}\varphi_{rq} - \omega_r \varphi_{rd}. \tag{16}$$

The air gap flux linkage:

$$\varphi_{sd} = L_s i_{sd} + L_m i_{rd}, \tag{17}$$

$$\varphi_{sq} = L_s i_{sq} + L_m i_{rq}, \tag{18}$$

$$\varphi_{rd} = L_r i_{rd} + L_m i_{sd}, \tag{19}$$

$$\varphi_{rq} = L_r i_{rq} + L_m i_{sq}, \tag{20}$$

with

$$L_s = L_m + L_{ls}; \quad L_r = L_m + L_{lr},$$

where L_m is magnetizing inductance, L_{ls} and L_{lr} are leakage inductance per phase.

The excitation system is formed by a bank of the excitation capacitor delta connected. The capacitance value is selected to generate the rated voltage at no-load. Components of the stator voltage v_{sd} and v_{sq} as state variables are given by:

$$\frac{\mathrm{d}v_{sd}}{\mathrm{d}t} = \frac{1}{C} i_{cd}, \tag{21}$$

$$\frac{\mathrm{d}v_{sq}}{\mathrm{d}t} = \frac{1}{C} i_{cq}, \tag{22}$$

where C is excitation capacitance [F].

The electromagnetic torque of the induction generator can be expressed as a function of d and q axes stator and rotor currents as:

$$T_e = \frac{3}{2} p L_m (i_{sq} i_{rd} - i_{sd} i_{rq}). \tag{23}$$

The magnetizing inductance L_m is obtained from the no load test at synchronous speed. The no load characteristic is given in Appendix.

The drive train of the SEIG is one mass model and the mechanical equation can be written as:

$$J\frac{\mathrm{d}\Omega_g}{\mathrm{d}t}=\frac{\eta}{G}T_t-T_e, \tag{24}$$

where J is the equivalent rotor inertia rendered at the high speed shaft [kgm²], and η is gear box efficiency.

5.3 Modelling of the voltage frequency controller

As shown in Fig. 4 the main parts of the VFC are voltage sourced converter (VSC) with an isolated transformer and LC filter at its AC side and a BESS at its DC link side. The VSC consists of 6 insulated gate bipolar-junction transistors (IGBT). The SVPWM technique is used in order to generate the gating signals for IGBTs. As described in Section 3, upon the modulation index value, the VFC manages the power flow among the SEIG, the BESS and loads to maintain terminal voltage and frequency constant, Fig. 4. The modulation index is synthesized by a PI controller of the single voltage closed loop control. Assuming the instantaneous line voltage at the SEIG terminals (v_a, v_b, v_c) are sinusoidal then the magnitude of the AC voltage is given by:

$$|V_G|=\sqrt{\frac{2}{3}(v_a^2+v_b^2+v_c^2)}\,. \tag{25}$$

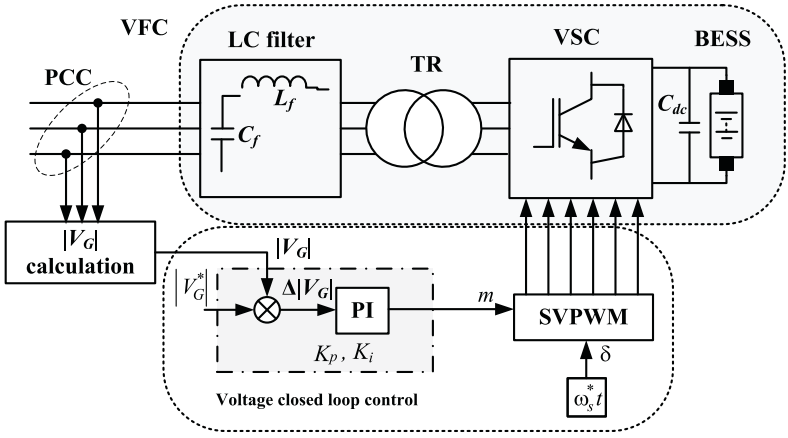

Fig. 4 – *Schematic diagram of the voltage frequency controller.*

The AC voltage error at a k^{th} sampling time is given by:

$$\Delta V_G(k)=\left|V_G^*\right|(k)-\left|V_G\right|(k), \tag{26}$$

where $|V_G^*|(k)$ is the magnitude of reference AC voltage. The output of the PI controller 'm' for maintaining constant AC terminal voltage at the k^{th} sampling time is expressed as:

$$m(k)=m(k-1)+K_p\left[\Delta V_G(k)-\Delta V_G(k-1)\right]+K_i\Delta V_G(k), \tag{27}$$

where K_p and K_i are the proportional and the integral gain constants of the PI controller. The load angle 'δ' (Section 3) is set to the nominal frequency, so no frequency control is needed and SEIG frequency follows the VSC set frequency in spite of perturbations.

The battery used as a backup for the SEIG is a lead acid battery, which can relatively maintain a large specific power, so, they have the ability to supply high surge currents. The equivalent circuit of the battery based model [23] is pictured in Fig. 5. It consists of an internal resistance R_{in} and a battery. The value of the battery's EMF, E, varies directly with the state-of-charge 'SOC'.

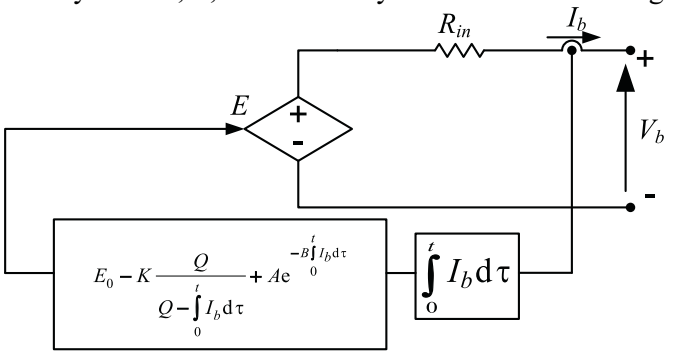

Fig. 5 – *Equivalent circuit of the battery model.*

where:

$$\mathrm{SOC}\,\% = 100\left(1 - \frac{\int_0^t I_b \,\mathrm{d}\tau}{Q}\right), \tag{28}$$

I_b – current discharge [A];

Q – the battery capacity [Ah].

The EMF is expressed as follows:

$$E = E_0 - K\frac{Q}{Q - \int_0^t I_b \,\mathrm{d}\tau} + A\mathrm{e}^{\left(-B\int_0^t I_b \,\mathrm{d}\tau\right)}, \tag{29}$$

where:

E – battery open-circuit voltage [V];

E_0 – battery constant voltage [V];

A – exponential voltage [V];

B – exponential capacity [Ah^{-1}];

K – polarisation voltage [V].

Values of battery's parameters are given in the Appendix. This model requires just a few parameters given by the manufacturer's datasheet. The discharge curve of the battery applied in the simulation is shown in Fig. 6, which was obtained using the described model.

The terminal voltage at DC link is computed as:

$$V_b = E - R_{in} I_b \,. \tag{30}$$

The constant voltage E_0 must be greater than the RMS value of the line voltage for satisfactory the PWM principle as [18]:

$$E_0 > \left(\frac{2}{m} \sqrt{\frac{2}{3}} k V_{Gl-l} \right) = \frac{1.633}{m} k V_{Gl-l} \,, \tag{31}$$

where VGl-l is RMS value of the line voltage on the AC side of the converter, E0 is selected as 240 V, and k is the coupling transformer turns ratio.

For the filter design a variety of optimization criteria exist such as minimum cost, losses, volume and weight. The selection was chosen to fulfil IEEE-SCR 20-50 recommendation [24]. The values of LC-filter components, for PWM converter at 10 kHz switching frequency, in order to attenuate the switching harmonics below IEEE-SCR 20-50 limits, are given in Appendix.

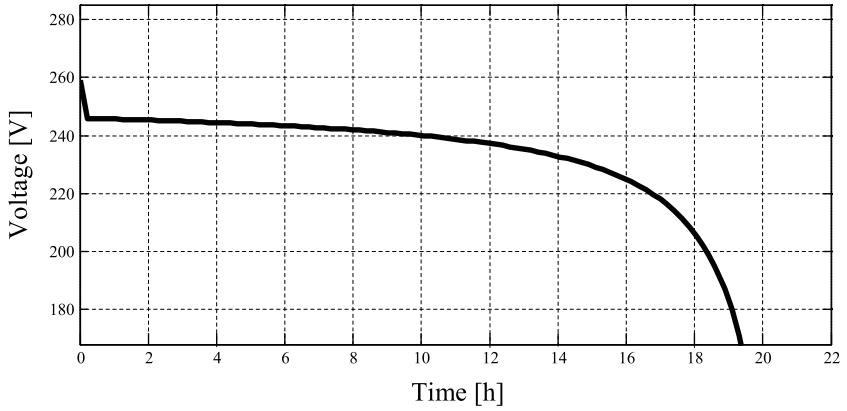

Fig. 6 – *Battery discharge curve with a constant current of* 20A.

5.4 Modelling of the consumer loads

The consumer loads consisting of a balanced R-L load (static load) modelled in PSB using three-phase series RLC load star connected. The dynamic load is a squirrel cage IM; the model is similar to the induction generator but its parameters are related to the motor. The IM is started at rated load torque and the effect of the saturation is not taken into account.

6 Simulation Results and Analysis

In order to verify the effectiveness of the proposed VFC for autonomous SEIG, a simulation was carried out in the MATLAB/Simulink® environment as shown in Fig. 7. The system simulation parameters are listed in the Appendix.

In this investigation, different perturbations have been applied to the WPCS at regular instants of 0.4 s to demonstrate the capability of the controller as a voltage and frequency regulator.

Initially, no load is connected to the generator terminals and the VFC is connected to the PCC. According to turbine characteristics and to C_p versus TSR curve, for 11 m/s wind speed, the mechanical power is 7.5 kW. Because of the SEIG and gear box losses, the wind turbine output power is slightly lower than the rated power. The SEIG reactive power demand is only provided by the capacitor bank, thus the VFC reactive power is zero. All the SEIG generated active power is absorbed by the VFC and stored in BESS as shown in Figs. 10 and 11. So, a power balance is realized. The magnitude value |VG| in steady-state reaches 326.5 V and the frequency is held constant at 50 Hz as presented in Fig. 8.

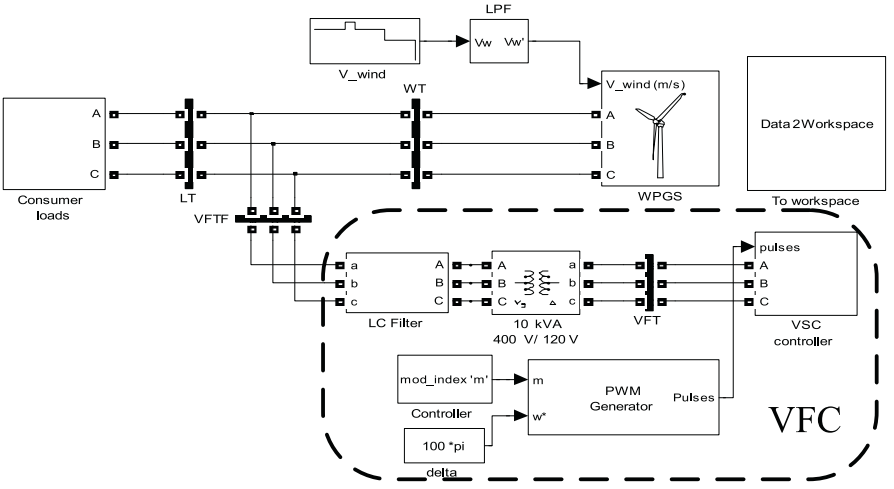

Fig. 7 – *Simulation circuit of the proposed wind power generating system.*

The simulation transient curves are respectively from Figs. 8–11, the voltage at PCC (V_{PCC}), the frequency at PCC (f_{PCC}), turbine active power (P_{turb}), generator active power (P_{gen}), load active power (Pload), VFC active power (P_{conv}), capacitor reactive power (Q_{cap}), reactive power at PCC (Q_{PCC}), load reactive power (Q_{load}), VFC reactive power (Q_{conv}), battery voltage (V_{batt}) and current (I_{batt}).

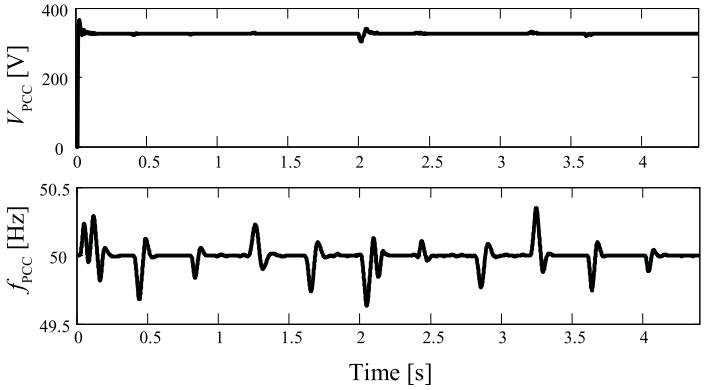

Fig. 8 – *Peak terminal voltage and frequency at* PCC.

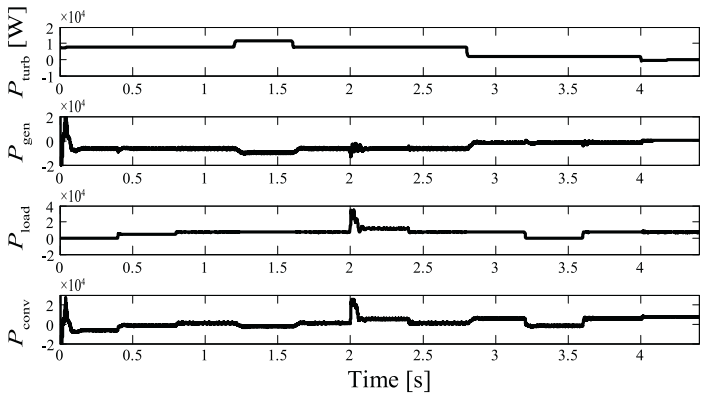

Fig. 9 – *Active power flow of power generating system.*

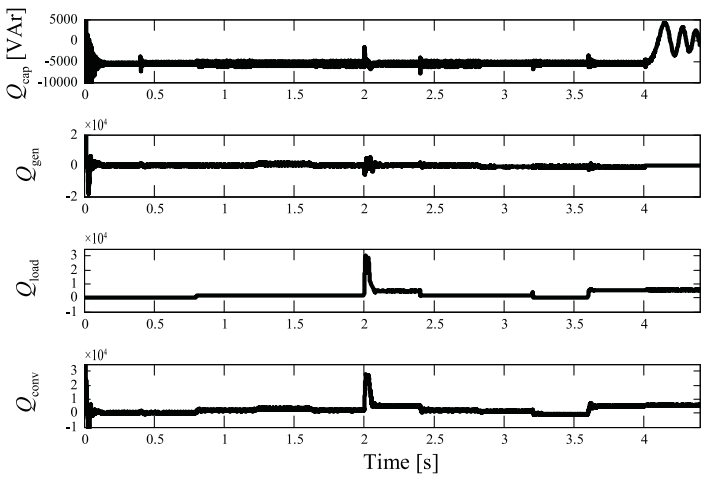

Fig. 10 – *Reactive power flow of power generating system.*

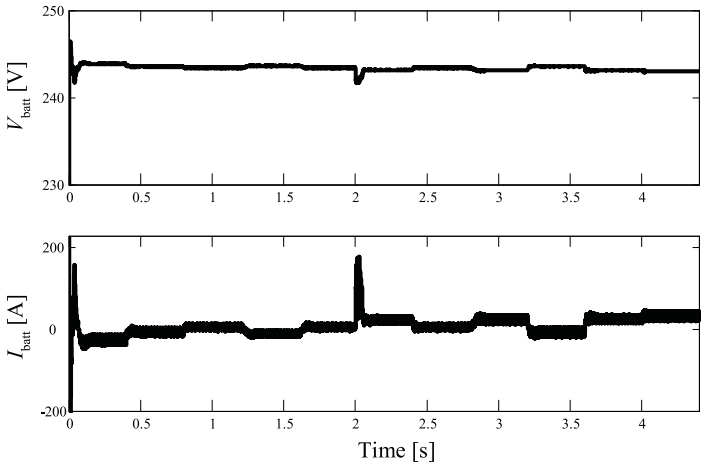

Fig. 11 – *Battery voltage and current during charge and discharge.*

At $t = 0.4$ s, a resistive load $P_{load} = 5$ kW is connected across the PCC, the magnitude voltage |VG| falls, and the frequency decrease. The active power drawn by the VFC is decreased to ensure the power balance at PCC. Since, the reactive power of the capacitor bank is enough for SEIG magnetization. Thus, the voltage remains constant. The VFC reactive power is always zero, the BESS absorbs the excess active power to maintain the system frequency constant as shown in Figs. 8–11.

At $t = 0.8$ s, a secondary load with active and reactive components is connected, $P_{load} = 2.5$ kW; $Q_{load} = 1.875$ kVAr. The total load active/reactive power becomes $P_{load} = 7.5$ kW and $Q_{load} = 1.875$ kVAr. For the sudden load reactive power demand, the voltage |VG| goes down. The VFC supplies the reactive power to the load to maintain the terminal voltage constant. During steady-state operation Q_{load} is approximately equal Q_{conv}. On the other hand, the total load active power is provided by the generator and P_{conv} becomes zero, as stated in Figs. 9 and 10. So, the frequency is maintained constant as shown in Fig. 8.

At $t = 1.2$ s, the wind speed is raised to 13 m/s, and the generated power P_{gen} is greater than the rated power as shown in Fig. 9. This kind of perturbation leads to a rise of the frequency due the excessive mechanical power. Since the power generated is more than the load active power demand, the BESS is absorbing the surplus power to maintain the terminal voltage and frequency constant under steady-state shown in Figs. 8 – 11.

At $t = 1.6$ s, the wind speed is rendered at 11 m/s. Since the load has not changed, this case is analogous to the case where speed was 11 m/s before its increase (i.e. at $t = 0.8$ s).

At $t = 2$ s, an induction motor is connected across the PCC. At start moment an inrush active/reactive power is drawn by the motor. The load active power is very larger than P_{gen}, as a consequence, the frequency falls. Moreover, since, the required reactive power of the load is very high, the voltage droop is very significant. It can be observed from Fig. 10 that due the dip in terminal voltage, the SEIG and capacitor bank reactive power decrease. The VFC tries to supply the required load active/reactive power to keep the terminal voltage and frequency constant, the BESS is in discharging mode. Due the motor inertia, the voltage dip recovers in few cycles, after the transient die away. In the steady-state, Pconv is approximately equal to the different active power between Plaod and Pgen, and the VFC supplies Q_{load} as depicted in Figs. 9 and 10.

At $t = 2.4$ s, the induction motor is disconnected to the PCC. The WPCS reacts in a similar way as stated at $t = 1.6$ s. The VFC supplies solely the reactive power to the load. The induction motor disconnection leads to a momentary rise in frequency and the terminal voltage tries to go up, but due the VFC closed-loop control |VG| decreases and holds at the reference value.

At $t = 2.8$ s, the wind speed is reduced to 8 m/s. The frequency fall is due to the reduced Pgen. Consequently, the BESS supplies the needed active power to compensate the fall in wind turbine output power Fig. 9. So, the frequency becomes equal to the VFC set frequency. In the same time the SEIG reactive power falls, Fig. 10, also the VFC reactive power decreases, but the voltage is held close to its desired level as shown in Fig. 8. The VFC still supplies reactive power to the SEIG and load.

At $t = 3.2$ s, the load is removed from the PCC. The variation of loads leads to the momentary rise in system frequency due to Pgen excesses P_{load}. As a result, the BESS is absorbing the surplus power. The terminal voltage rises slightly. In this state the VFC reacts as an inductive load and absorbs the excess active /reactive power, the BESS is in charging mode Fig. 10. This case is similar to the initial case, but for wind speed 8 m/s, in which the absorbed active power is less than the rated power. Figs. 8–11.

At $t = 3.6$ s, a rated balanced three phase load ($P_{load} = 7.5$ kW; $Q_{load} = 5.625$ kVAr) is connected across the SEIG terminals. This perturbation leads to a momentary fall in the SEIG terminal voltage and frequency. Because, the generated active power by the SEIG is less than to the rated power (i.e $V_w = 8$ m/s), the VFC reacts as a source and supplies the deficit of active power to the load, the BESS is in discharging mode Fig. 10. In a similar manner, the load reactive power demand is assured by the VFC. Under steady-state, the terminal voltage and frequency reaches their desired values.

Finally, at $t = 4$ s, a fall in wind speed in which: $V_w = 2$ m/s; $V_w < V_{w\,cut\_in}$ is applied. This speed perturbation leads to a momentary fall in the voltage and frequency at the PCC. For security purposes, the generator is isolated from the PCC, so the load is only connected to the PCC. In order to maintain constant

voltage and frequency at the PCC, the rated active/reactive power of the load is therefore provided by the VFC, the BESS is in discharging mode, the frequency is restored to the VFC set frequency. Under these operating conditions, the VFC remains to supply the load for a few hours until a tolerable 'SOC' or a new wind speed greater than $V_{\text{w cut in}}$ appears again.

7 Conclusion

In this investigation, a control strategy for controlling the SEIG terminal voltage and frequency has been presented. The VFC consists of three-level neutral clamped voltage sourced converter along with BESS on its DC link. The VFC set frequency is imposed so; a voltage single closed loop control is used to maintain both voltage and frequency close to their desired values. Under several balanced loads and speed perturbations, the simulation results show the effect of perturbations on active/reactive power direction, SEIG terminal voltage and frequency. In each case the VFC has been found suitable with single-loop control to regulate the voltage and frequency and behaves as a free-slack to adequately manage power flow. The proposed wind power generating system can be used in the isolated rural, ships and mountainous areas far from the conventional sources. We are currently working on the capability of the VFC as a harmonic eliminator and a load balancer/leveller when the SEIG operates in asymmetric modes.

8 Appendix

SEIG:

7.5 kW, 400 V, 50 Hz, Y-connected 4-pole,
$R_s = 0.7384\ \Omega$, $R_r = 0.7402\ \Omega$, $L_{ls} = L_{lr} = 3.045$ mH, $J_g = 0.034$ kgm^2,
the no load RMS line voltage curve versus the armature current:

$$V_{G1\text{–}1}(I_{s\_peak}) = 0.16I_{s\_peak}^3 - 7.17I_{s\_peak}^2 + 105.2I_{s\_peak} - 31.2\,.$$

Excitation capacitance:

$Q_c = 5.6$ kVAr, delta connected.

Wind turbine:

7.5 kW, $V_{\text{w cut-in}} = 3$ m/s, $J_t = 3$ kgm^2, rated wind speed $V_w = 11$ m/s,
$C_1 = 0.5176$, $C_2 = 116$, $C_3 = 0.4$, $C_4 = 5$, $C_5 = 21$, $C_6 = 0.0068$.

VFC:

$L_f = 2.5$ mH, $R_f = 0.01\ \Omega$, $C_f = 33\ \mu$F, $C_{dc} = 5000\ \mu$F,
$K_p = 0.007$, $K_i = 0.4$, $E_{bat} = 240$ V.

BESS:

$E_0 = 252{,}9$ V, $R_{in} = 0.015\ \Omega$, $K = 6.6$ V, $A = 13.2$ V,
$B = 9.375\ (\text{Ah})^{-1}$, $Q = 200$ Ah.

IM:

4 kW, cosφ = 0.8, 400 V, 50 Hz, 1430 rpm, T_N = 25 Nm,
R_s = 1.405 Ω, R_r = 1.395 Ω, L_{ls} = L_{lr} = 5.84 mH, L_m = 0.1722 H,
J = 0.013 kgm^2, B = 0.00298 Nms.

9 References

[1] B. Singh, G.K. Kasal: Analysis and Design of Voltage and Frequency Controllers for Isolated Asynchronous Generators in Constant Power Applications, IEEE International Conference on Power Electronics Drives and Energy Systems, New Delhi, India, 12 – 15 Dec. 2006.

[2] S. Heier: Grid Integration of Wind Energy Conversion Systems, John Willey and Sons, Chichester, UK, 2006.

[3] E.G. Marra, J.A. Pomilio.: Self–excited Induction Generator Controlled by a VS-PWM Bidirectional Converter for Rural Application, IEEE Transaction on Industry Applications, Vol. 35, No. 4, July/Aug. 1999, pp. 877 – 883.

[4] R. Rabinovici, A. Kuperman.: Autonomous Induction Generator with Solid-state Reactive Power Excitation, 22nd Convention of Electrical and Electronics Engineers in Israel, Beer-Sheva, Israel, 01 Dec. 2002, pp. 47 – 49.

[5] E. Muljadi, J. Sallan, M. Sanz, C.P. Butterfield: Investigation of Self-excited Induction Generators for Wind Turbine Applications, 34th Industry Application Conference, Phoenix, AZ, USA, 03 – 07 Oct. 1999, Vol. 1, pp. 509 – 515.

[6] J. Faiz.: Design and Implementation of a Solid-state Controller for Regulation of Output Voltage of a Wind Driven Self-excited Three Phase Squirrel Cage Induction Generator; 8th International Conference on Electrical Machines and Power Systems, Nanjing, Jiangsu, China, 29 Sept. 2005, Vol. 3, pp. 2384 – 2388.

[7] A. Nesba, R Ibtiouen, O. Touhami.: Dynamic Performances of Self-excited Induction Generator Feeding Different Static Loads, Serbian Journal of Electrical Engineering, June 2006, Vol. 3, No. 1, pp 63 – 67.

[8] T. Ahmed, E. Hiraki, M. Nakaoka, O. Noro: Three-phase Self-excited Induction Generator Driven by Variable-speed Prime Mover for Clean Renewable Energy Utilizations and its Terminal Voltage Regulation Characteristics by Static VAR Compensator, 38th Industry Application Conference, Salt Lake City, UT, USA, 12 – 16 Oct. 2003, Vol. 2, pp. 693 – 700.

[9] S. Wekhande, V. Agarwal.: Simple Control for a Wind Driven Induction Generator, IEEE Industry Application Magazine, Vol. 7, No. 2, March/April 2001, pp. 44 – 53.

[10] S.C. Kuo, L. Wang: Analysis of Voltage Control for a Self-excited Induction Generator using a Current-controlled Voltage Source Inverter (CC-VSI), IEE Proceeding – Generation, Transmission and Distribution, Vol. 148, No. 5, Sept. 2001, pp. 431 – 438.

[11] B. Singh, L. B. Shilpakar.: Analysis of a Novel Solid State Voltage Regulator for a Self-excited Induction Generator, IEE Proceeding – Generation, Transmission and Distribution, Vol. 145, No. 6, Nov. 1998, pp. 647 – 655.

[12] A.M. Sharaf, S.K. Murugan.: Dynamic Power Filter and Capacitor Compensator for Isolated Self-excited Induction Generator Driven by a Wind Turbine, 11th International Conference on Harmonics and Quality of Power, Lake Placid, NY, USA, 12 – 15 Sep. 2004, pp. 46 – 49.

[13] D. Joshi, K.S. Sandhu, M.K. Soni.: Constant Voltage Constant Frequency Operation for a Self-excited Induction Generator, IEEE Transaction on Energy Conversion, Vol. 21, No. 1, March 2006, pp. 228 – 234.

[14] B. Singh, G.K. Kasal: Voltage and Frequency Controller for a Three-phase Four-wire Autonomous Wind Energy Conversion System, IEEE Transaction on Energy Conversion, Vol. 23, No. 2, June 2008, pp. 509 – 518.

[15] B. Singh, S. Sharma.: Power Balance Theory based Voltage and Frequency Control for IAG in Wind Power Generation, 2nd International Conference on Emerging Trends in Engineering and Technology, Nagpur, Maharashtra, India, 16 – 18 Dec. 2009, pp. 40 – 45.

[16] B. Singh, S.S. Murthy, S. Gupta.: A Voltage and Frequency Controller for Self-excited Induction Generators, Electric Power Components and Systems, Vol. 34, No. 2, Feb. 2006, pp. 141 – 157.

[17] G.K. Kasal, B. Singh: Decoupled Voltage and Frequency Controller for Isolated Asynchronous Generators Feeding Three-phase Four-wire Loads, IEEE Transaction on Power Delivery, Vol. 23, No 2, April. 2008, pp. 966 – 973.

[18] B. Singh, G.K. Kasal: Battery Energy Storage System based Controller for a Wind Turbine Driven Isolated Asynchronous Generator, Journal of Power Electronics, Vol. 8, No. 1, Jan. 2008, pp. 81 – 90.

[19] A. Benlamoudi, R. Abdessemed: STATCOM based Voltage-frequency Regulation for SEIG Driven by an Uncontrolled Speed Turbine, International Journal of Power and Energy Conversion, Vol. 1, No. 4, Oct. 2009, pp. 399 – 416.

[20] J.K. Chatterjee, B.V. Perumal, N.R. Gopu: Analysis of Operation of Self-excited Induction Generator with Generalized Impedance Controller, IEEE Transaction on Energy Conversion, Vol. 22, No. 2, June 2007, pp. 307 – 315.

[21] B.V. Perumal, J.K. Chatterjee: Voltage and Frequency Control of a Stand-alone Brushless Wind Electric Generation using Generalized Impedance Controller, IEEE Transaction on Energy Conversion, Vol. 23, No. 2, June 2008, pp. 632 – 641.

[22] K. De Brabandere, B. Bolsens, J. Van den Keybus, A. Woyte, J. Driesen, R. Belmans: A Voltage and Frequency Droop Control Method for Parallel Inverters, IEEE Transaction on Power Electronics, Vol. 22, No. 4, July 2004, pp. 1107 – 1115.

[23] O. Tremblay, L.A. Dessaint, A.I. Dekkiche: A Generic Battery Model for the Dynamic Ssimulation of Hybrid Electric Vehicles, Vehicle Power and Propulsion Conference, Arlington, TX, USA, 09 – 12 Sep. 2007, pp. 284 – 289.

[24] IEEE Standard 519-1992: IEEE Recommended Practices and Requirements for Harmonic Control in Electrical Power Systems, New York, USA, 1993.